sustainability

MDPI

Article

Assessing the Viability of GeO_2/GeO Redox Thermochemical Cycle for Converting CO_2 into Solar Fuels

Rahul R. Bhosale *, Shelby Adams, Zachary Allen, Gabrielle Bennett, Edvinas Berezniovas, Taylor Bishop, Michael Bonnema, Sequoia Clutter, Ryan Fagan, Jordan Halabrin, Mason Hobbs, Daniel Hunt, Miguel Ivarra, Mattigan Jordan, Pooja Karunanithi, Julianna Mcreynolds, Valerie Ring, Samuel Smith and Jonathan West

Department of Chemical Engineering, University of Tennessee, 615 Mccallie Ave, Chattanooga, TN 37403, USA; zlx374@mocs.utc.edu (S.A.); rgh377@mocs.utc.edu (Z.A.); kvy982@mocs.utc.edu (G.B.); nnr886@mocs.utc.edu (E.B.); twx738@mocs.utc.edu (M.B.); mxh589@mocs.utc.edu (S.C.); sqs167@mocs.utc.edu (R.F.); mjd588@mocs.utc.edu (J.H.); gql391@mocs.utc.edu (M.H.); cdd659@mocs.utc.edu (D.H.); dsr216@mocs.utc.edu (M.I.); wjg766@mocs.utc.edu (M.J.); jsp833@mocs.utc.edu (P.K.); qvt556@mocs.utc.edu (J.M.); yhp264@mocs.utc.edu (V.R.); wjk682@mocs.utc.edu (S.S.); jbj479@mocs.utc.edu (J.W.)

* Correspondence: rahul-bhosale@utc.edu or rrbhosle1985@gmail.com; Tel.: +1-(423)-425-5455

Abstract: The solar thermochemical process of splitting CO_2, known as CDS, is studied here using a redox cycle involving GeO_2/GeO. The required thermodynamic data for a second-law-efficiency analysis is obtained from the HSC Chemistry software. The goal of this study is to investigate how different parameters, such as the operating temperatures and molar flow rate of the inert sweep gas, as well as the inclusion of separation units, heat exchangers, heaters, and coolers, can affect the solar-to-fuel energy conversion efficiency of the GeO_2/GeO cycle. All calculations assume a constant gas-to-gas heat recovery effectiveness of 0.5. The analysis shows that the solar-to-fuel energy conversion efficiency is lower at a thermal reduction temperature of 1600 K (11.9%) compared to 2000 K. This is because high energy duties are required for heater-2, heater-3, and separator-1 due to the need for a higher inert gas flow rate. After conducting a comparative analysis of the three CDS cycles, it can be inferred that the GeO_2/GeO cycle exhibits a significantly higher solar-to-fuel energy conversion efficiency in comparison to the ZnO/Zn and SnO_2/SnO cycles across all thermal reduction temperatures. According to the comparison, it is confirmed that the GeO_2/GeO CDS cycle can achieve a reasonably high solar-to-fuel energy conversion efficiency of 10% at less than 1600 K. On the other hand, ZnO/Zn and SnO_2/SnO CDS cycles require a thermal reduction temperature of more than 1850 K to achieve a solar-to-fuel energy conversion efficiency of 10%.

Keywords: GeO_2/GeO cycle; CO_2 splitting; solar fuels; thermodynamic model; efficiency

Citation: Bhosale, R.R.; Adams, S.; Allen, Z.; Bennett, G.; Berezniovas, E.; Bishop, T.; Bonnema, M.; Clutter, S.; Fagan, R.; Halabrin, J.; et al. Assessing the Viability of GeO_2/GeO Redox Thermochemical Cycle for Converting CO_2 into Solar Fuels. *Sustainability* **2024**, *16*, 2553. https://doi.org/10.3390/su16062553

Academic Editor: Andrea Colantoni

Received: 2 March 2024
Revised: 10 March 2024
Accepted: 15 March 2024
Published: 20 March 2024

1. Introduction

Harnessing the potential of solar energy for fuel production can be achieved through the use of concentrated solar power to drive chemical reactions. This method offers a promising option for utilizing the abundant solar energy available and converting it into a reliable source of fuel. Several researchers have conducted a thorough investigation of a solar-driven thermochemical redox cycle that utilizes metal oxide (MO) in the process of splitting H_2O/CO_2. The main objective of this cycle is to produce H_2 gas through the thermochemical H_2O-splitting (WS) reaction, which is driven by solar power. The H_2 produced from this reaction can be used directly as a fuel with ease. One alternative approach to producing energy is through the use of solar CO generated via the thermochemical CO_2-splitting (CDS) reaction. This approach involves the combination of solar CO with H_2 to synthesize solar syngas [1]. One of the key benefits of this method is that it helps to reduce the dangerous consequences of CO_2 emissions [2] by recycling it into a chemical fuel. In addition, the use of solar thermochemical CDS can provide a more sustainable

and eco-friendly solution to energy production. Extensive research has been conducted on various MOs for solar thermochemical cycles, including Fe_3O_4/FeO [3,4], ZnO/Zn [5], SnO_2/SnO [6], ferrites [7], doped ceria [8,9], and perovskite [10,11] materials. Two prestigious European institutions from Switzerland and France have paid special attention to the ZnO/Zn and SnO_2/SnO cycles. The ZnO/Zn-based redox system has been studied extensively by the Paul Scherrer Institute in Switzerland [12], whereas the SnO_2/SnO-based redox cycle has been considerably investigated by PROMES-CNRS in France [13].

During the early years of the ZnO/Zn cycle (before 2005), the main focus was on (a) using solar thermal energy to decompose ZnO [14], (b) studying the crystallization and condensation of Zn with variations in O_2 concentration [15], (c) analyzing the kinetics of the thermal reduction (TR) of ZnO [16], (d) evaluating the economics of the ZnO/Zn cycle [17], and (e) designing solar reactors suitable for this process [18]. After 2005, application of an aerosol reactor for the Zn hydrolysis [19,20], thermal decomposition of ZnO in a fluid wall reactor [21], the kinetics of the WS and combined WS + CDS using a thermogravimetric analyzer [22,23], and application of a 10 kW solar reactor for the TR of ZnO [24] were investigated. A team of researchers from ETH Zurich and the Paul Scherrer Institute recently conducted two experimental campaigns to test a pilot-scale 100 kW solar reactor for the thermal decomposition of ZnO [25,26]. The tests were conducted using a 1 MW solar furnace at PROMES-CNRS, France.

In the case of the SnO_2/SnO redox cycle, Abanades et al. [27] reported that SnO_2 needs to be heated to a temperature above 1873 K at atmospheric pressure to undergo thermal decomposition into SnO. Charvin et al. [13] estimated the activation energy of SnO_2 thermal decomposition as 394.8 kJ/mol using thermogravimetry. Chambon et al. [28] studied the kinetics of SnO_2/SnO-driven WS and determined the order to be one and the activation energy to be 122 kJ/mol. Chambon et al. [29] conducted an in-depth analysis of the recombination process of SnO and O_2, which occurs during the quenching step. Abanades et al. [30] conducted a study to investigate the effectiveness of utilizing the SnO_2/SnO redox cycle for a combined WS and CDS process by using a thermogravimetric analyzer.

Although the redox cycles of ZnO/Zn and SnO_2/SnO have been extensively investigated, researchers in the solar thermochemical community are seeking a more energy-efficient redox cycle. There is an option available in this category called the GeO_2/GeO redox cycle. In 2009, Kang et al. [31] investigated the GeO_2/GeO WS cycle and found that the requirement of the TR temperature (T_{red}) was lower for the GeO_2/GeO cycle than for the ZnO/Zn and SnO_2/SnO cycles. The authors further reported that the process efficiency associated with the GeO_2/GeO WS cycle was higher compared to the ZnO/Zn and SnO_2/SnO WS cycles. Recently, Bhosale [32] conducted a thermodynamic study of the GeO_2/GeO WS cycle. He estimated process parameters as a function of O_2 partial pressure, TR, and WS temperatures.

In this study, Bhosale and his team of undergraduate researchers develop a thermodynamic model for the CDS redox cycle based on GeO_2/GeO. Various process parameters are calculated by considering different temperatures, molar flow rates of inert sweep gas ($\dot{n}_{inert}$), and the inclusion of gas separators, heat exchangers, heaters, coolers, and fuel cell for determining the solar-to-fuel energy conversion efficiency ($\eta_{solar-to-fuel}$). At the end of the study, a detailed comparison is provided between three redox CDS cycles: GeO_2/GeO, ZnO/Zn, and SnO_2/SnO. The comparison is based on $\eta_{solar-to-fuel}$.

2. Thermodynamic Model

The process of generating CO through the solar-driven GeO_2/GeO-based CDS redox cycle involves two steps, as described in the following reactions.

$$GeO_2 \rightarrow GeO + \frac{1}{2}O_2 \quad (1)$$

$$GeO + CO_2 \rightarrow GeO_2 + CO \quad (2)$$

The model presented in Figure 1 was used to examine the thermodynamic feasibility of the GeO_2/GeO-based CDS redox cycle. The thermodynamic model operates under the assumption that the gas behaves ideally and the system is in a steady state. The processes of thermal reduction and CDS reaction are carried out in two separate cells, one for reduction and the other for oxidation. Both cells are operated at a constant temperature, i.e., thermal reduction (T_{red}) and CDS temperature (T_{oxd}). The reduction cell operates at a higher temperature compared to the oxidation cell. During the GeO_2 decomposition process, a continuous $\dot{n}_{inert}$ (N_2) is employed to facilitate a reduction at T_{red}. The thermodynamic evaluation is carried out by maintaining a consistent flow of GeO_2, with a rate of 1 mole per second.

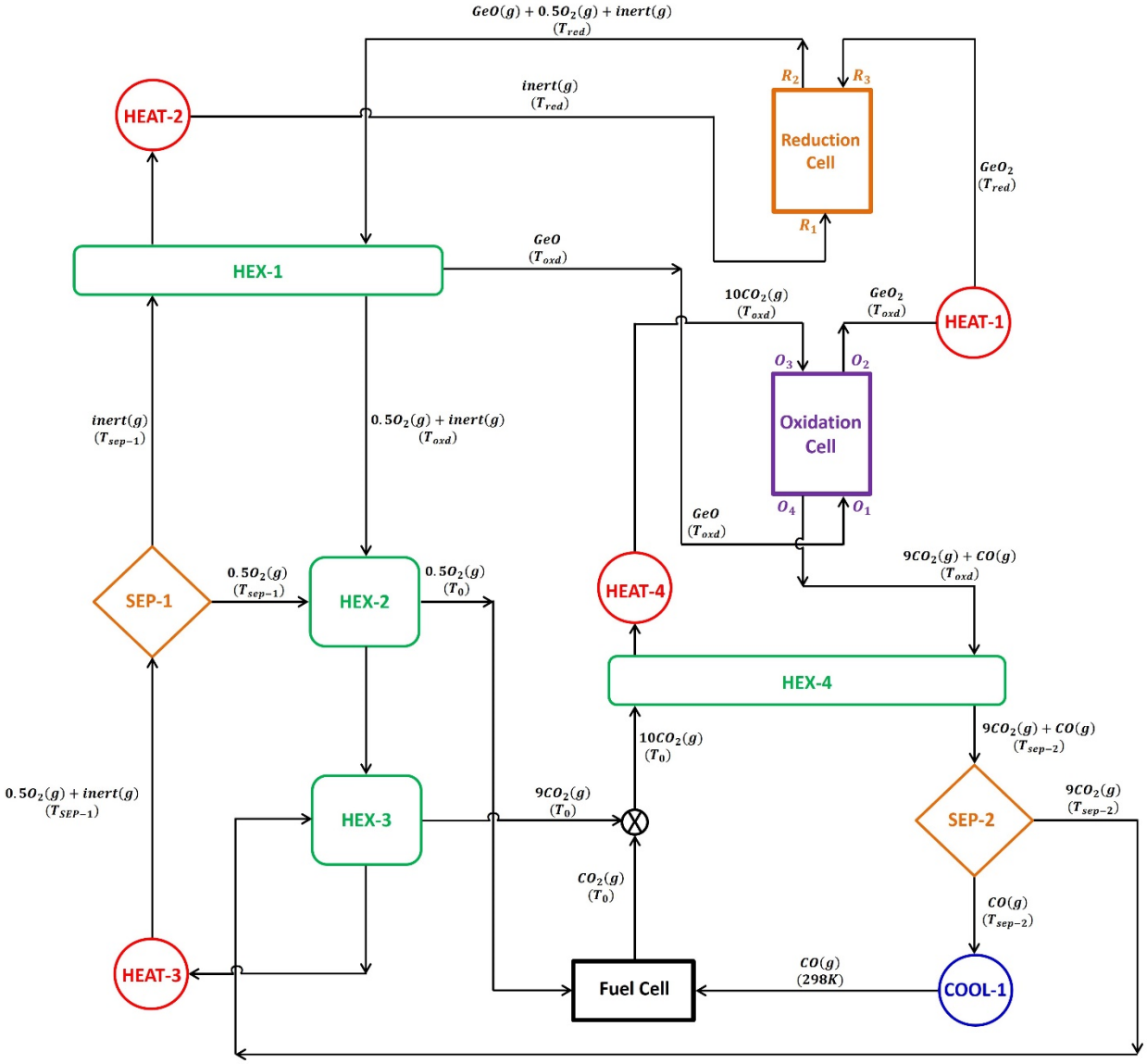

Figure 1. A process model of the GeO_2/GeO redox thermochemical cycle for CO_2 conversion into solar fuels.

After exiting from separator-1 and passing through heater-2, the recycled inert sweep gas stream and GeO_2 from the oxidation cell after CDS reaction enter the reduction cell where GeO_2 undergoes thermal decomposition. This results in the production of gaseous GeO and O_2. It is assumed that GeO_2 and the gaseous species have reached equilibrium.

Equation (3) is utilized to estimate the amount of energy needed for the thermal reduction of GeO_2.

$$\dot{Q}_{GeO_2-red} = \dot{n}_{GeO_2}\Delta H|_{GeO_2 \rightarrow GeO(g)+\frac{1}{2}O_2(g)} \quad (3)$$

To facilitate the removal of gaseous products, namely, GeO and O_2, from the reduction cell, an inert sweep gas is employed. The gas mixture, containing GeO, O_2, and inert sweep gas, is cooled below the melting point of GeO by using a gas-to-gas heat exchanger, HEX-1, to avoid the recombination of gaseous products at higher temperatures. The solid GeO is transferred from HEX-1 to the oxidation cell, where it is re-oxidized to GeO_2 at T_{oxd} through a CDS reaction. It is assumed that 100% conversion occurs during thermal reduction and CDS when evaluating the presented thermodynamic model.

To simulate the practical operation of an oxidation cell, CDS reactions use an excess of CO_2 of 10 times the stoichiometric requirement. As shown in Figure 1, CO_2 enters the oxidation cell at state O_3, while GeO enters at state O_1. After the re-oxidation reaction, GeO exits the oxidation cell as state O_2, while any remaining CO_2 and produced CO gases exit as a mixture at state O_4. As the CDS reaction is exothermic, the energy released by the oxidation cell is estimated using the following formula:

$$\dot{Q}_{GeO-oxd} = -\dot{n}_{GeO_2}\Delta H|_{GeO+10CO_2(g) \rightarrow GeO_2+9CO_2(g)+CO(g)} \quad (4)$$

Furthermore, Equation (5) is applied to calculate the energy required to heat the GeO_2 from T_{oxd} to T_{red} with the help of heater-1.

$$\dot{Q}_{heater-1} = \dot{n}_{GeO_2}\Delta H|_{GeO_2@T_{oxd} \rightarrow GeO_2@T_{red}} \quad (5)$$

Separator-2, which is operated at T_{sep-2} = 400 K, separates CO from unreacted CO_2. The operating efficiency of separator-2 is assumed to be 15%, with a 99.9% separation of CO from CO_2 [33]. Before entering separator-2, the CO_2/CO gas mixture is cooled from 1000 K to 400 K by passing through HEX-4. The required energy for achieving the desired separation is determined using the following equations:

$$\dot{Q}_{sep-2} = \dot{n}_{GeO_2}\left[\frac{T_{sep-2}}{\eta_{sep-2}}\left(\Delta S_{mix,O_4} - \Delta S_{mix,O_3}\right)\right] \quad (6)$$

$$\Delta S_{mix,O_3} = -R\left\{n_{CO_2}\ln\left(1-y_{CO,O_3}\right) + n_{CO,O_3} lny_{CO,O_3}\right\} \quad (7)$$

$$\Delta S_{mix,O_4} = -R\left\{n_{CO_2}\ln\left(1-y_{CO,O_4}\right) + n_{CO,O_4} lny_{CO,O_4}\right\} \quad (8)$$

The model incorporates a prototypical fuel cell that operates with 100% efficiency by utilizing CO and O_2 to complete the cycle. For the operation of this fuel cell, cooler-1 decreases the temperature of CO exiting separator-2 from 400 K to 298 K. The CO is consumed in the fuel cell, producing CO_2 that combines with unreacted CO_2 from HEX-3. This combined CO_2 stream is conveyed to the oxidation cell by passing through HEX-4 and heater-4. To find out the amount of energy needed to heat the CO_2, we use an energy balance calculation, which is presented below.

$$\dot{Q}_{CO_2-heat} = \varepsilon_{gg}\left[\dot{Q}_{(CO_2+CO)-cool}\right] + \dot{Q}_{heater-4} \quad (9)$$

$$\dot{Q}_{CO_2-heat} = \dot{n}_{CO_2}\Delta H|_{CO_2(g)@T_0 \rightarrow CO_2(g)@T_{oxd}} \quad (10)$$

$$\dot{Q}_{(CO_2+CO)-cool} = \dot{n}_{CO_2}\Delta H|_{CO_2(g)@T_{oxd} \rightarrow CO_2(g)@T_{sep-2}} + \dot{n}_{CO}\Delta H|_{CO(g)@T_{oxd} \rightarrow CO(g)@T_{sep-2}} \quad (11)$$

For the reduction and fuel cells to function smoothly, there needs to be a continuous and uninterrupted supply of inert gas and O_2. Recycling the inert gas that exits the reduction cell is crucial to improve the process's economics. Therefore, separator-1 is installed in the cycle to separate the inert gas and O_2, which exit the reduction cell as a

gas mixture, after performing the thermal decomposition of GeO_2. To achieve this gas separation, it is assumed that the ion transport membrane technology will be applied [34]. For the presented cycle, separator-1 is assumed to be operated at 1123 K with an efficiency of 15%. By passing the inert gas and O_2 mixture through HEX-2, HEX-3, and heater-3, it is heated because the operating temperature of separator-1 is higher than the CDS temperature. Below is the energy balance associated with these three units.

$$\dot{Q}_{(inert+O_2)-heat} = \varepsilon_{gg}\left[\dot{Q}_{O_2-cool} + \dot{Q}_{CO_2-cool}\right] + \dot{Q}_{heater-3} \tag{12}$$

Here,

$$\dot{Q}_{(inert+O_2)-heat} = \dot{n}_{inert}\Delta H|_{inert(g)@T_{oxd}\rightarrow inert(g)@T_{sep-1}} + \dot{n}_{O_2}\Delta H|_{O_2(g)@T_{oxd}\rightarrow O_2(g)@T_{sep-1}} \tag{13}$$

$$\dot{Q}_{O_2-cool} = \dot{n}_{O_2}\Delta H|_{O_2(g)@T_{sep-1}\rightarrow O_2(g)@T_0} \tag{14}$$

$$\dot{Q}_{CO_2-cool} = \dot{n}_{CO_2}\Delta H|_{CO_2(g)@T_{sep-2}\rightarrow CO_2(g)@T_0} \tag{15}$$

According to the second law of thermodynamics, the thermal energy required for separating the inert sweep gas and O_2 is computed using the entropy of mixing for each stream as follows [33]:

$$\dot{Q}_{sep-1} = \dot{n}_{GeO_2}\left[\frac{T_{sep-1}}{\eta_{sep-1}}\left(\Delta S_{mix,R_2} - \Delta S_{mix,R_1}\right)\right] \tag{16}$$

$$\Delta S_{mix,R_1} = -R\left\{n_{inert}\ln\left(1-y_{O_2,R_1}\right) + n_{O_2,R_1} ln y_{O_2,R_1}\right\} \tag{17}$$

$$\Delta S_{mix,R_2} = -R\left\{n_{inert}\ln\left(1-y_{O_2,R_2}\right) + n_{O_2,R_2} ln y_{O_2,R_2}\right\} \tag{18}$$

The O_2 that has been separated from the inert gas at 1123 K is cooled in HEX-2 to 298 K before being transferred to the fuel cell. In contrast, the inert sweep gas is heated from 1123 K up to T_{red} by passing through HEX-1 and heater-2. In HEX-1, the energy released during cooling of a gas mixture containing inert gas/O_2/GeO is used to heat the inert sweep gas. The heater-2 provides the additional energy required for the inert gas heating.

$$\dot{Q}_{inert-heat} = \varepsilon_{gg}\left[\dot{Q}_{(inert+O_2+GeO)-cool}\right] + \dot{Q}_{heater-2} \tag{19}$$

Here,

$$\dot{Q}_{inert-heat} = \dot{n}_{inert}\Delta H|_{inert(g)@T_{sep-1}\rightarrow inert(g)@T_{red}} \tag{20}$$

$$\dot{Q}_{(inert+O_2+GeO)-cool} = \dot{n}_{inert}\Delta H|_{inert(g)@T_{red}\rightarrow inert(g)@T_{oxd}} + \dot{n}_{O_2}\Delta H|_{O_2(g)@T_{red}\rightarrow O_2(g)@T_{oxd}} + \dot{n}_{GeO}\Delta H|_{GeO(g)@T_{red}\rightarrow GeO@T_{oxd}} \tag{21}$$

The efficiency of converting solar energy into fuel using the GeO_2/GeO CDS cycle can be calculated using the following equation:

$$\eta_{solar-to-fuel} = \frac{\dot{n}_{CO}\times HHV_{CO}}{\dot{Q}_{solar}} \tag{22}$$

where

$$\dot{Q}_{solar} = \frac{\dot{Q}_{TC}}{\eta_{absoption}} \tag{23}$$

$$\eta_{absorption} = 1 - \left(\frac{\sigma T_{red}^4}{IC}\right) \tag{24}$$

In order to determine the complete solar energy necessary for powering the cycle, it is essential to calculate the overall thermal energy required for performing the reactions as well as running the supplementary units, utilizing the following equation.

$$\dot{Q}_{TC} = \dot{Q}_{GeO_2-red} + \dot{Q}_{heater-1} + \dot{Q}_{heater-2} + \dot{Q}_{heater-3} + \dot{Q}_{heater-4} + \dot{Q}_{sep-1} + \dot{Q}_{sep-2} + \dot{Q}_{surf} \quad (25)$$

Here,

$$\dot{Q}_{surf} = 0.2 \times \dot{Q}_{GeO_2-red} \quad (26)$$

The re-radiation losses associated with the cycle are estimated as per the following equation:

$$\dot{Q}_{re-rad} = \eta_{absorption} \times \dot{Q}_{solar} \quad (27)$$

The values of the constant parameters used in this study are listed in Table 1.

Table 1. Values of each constant parameter used in the study.

Parameter	Value
T_{oxd}	1000 K
$\dot{n}_{GeO_2}$	1 mol/s
R	8.341 J/mol·K
T_0	298 K
T_{sep-1}	1123 K
T_{sep-2}	400 K
η_{sep-1}	15%
η_{sep-2}	15%
C	3000 suns
I	1000 W/m^2
σ	5.670×10^{-8} (W/m^2·K^4)
ε_{gg}	0.5

3. Results and Discussion

According to the published literature [22,29], achieving a cavity temperature in the range of 1600 K to 2000 K is feasible using concentrated solar power for a 100 kW solar reactor. The research teams from Switzerland [25,26] and Germany [35] have successfully demonstrated solar thermochemical reactions with reasonable energy efficiency despite the high temperatures required. Therefore, in this study, the thermodynamic model presented in Figure 1 is evaluated by varying the T_{red} from 1600 K to 2000 K, and by keeping ε_{gg} and T_{red} steady at 0.5 and 1000 K.

As a first step towards the estimation of the $\eta_{solar-to-fuel}$, it is crucial to estimate the $\dot{n}_{inert}$ needed for the complete thermal dissociation of GeO_2 in the temperature range selected for the T_{red}. By performing the equilibrium composition analysis using the HSC Chemistry software and its database, the variation in the $\dot{n}_{inert}$ as a function of the change in the T_{red} is estimated. The results obtained are reported in Figure 2. According to the results obtained, the need for $\dot{n}_{inert}$ to achieve 100% thermal reduction of GeO_2 reduces as the T_{red} increase from 1600 K to 2000 K. As the T_{red} increases from 1600 K to 1800 K and 2000 K, the $\dot{n}_{inert}$ needed decreases from 100 mol/s to 44 mol/s and 4 mol/s, respectively.

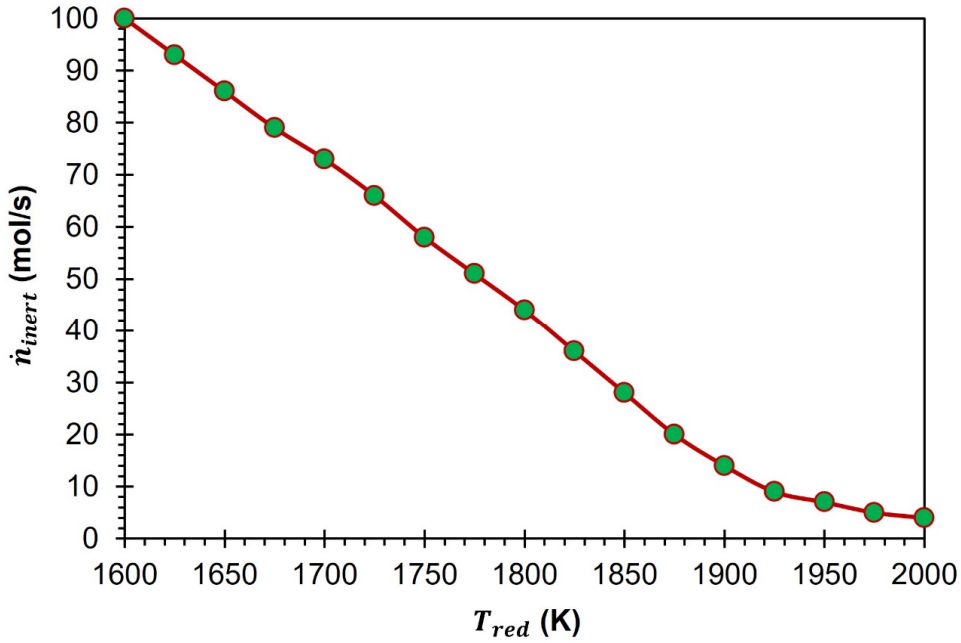

Figure 2. $\dot{n}_{inert}$ needed for the complete reduction of GeO_2 at T_{red} in the range of 1600 to 2000 K.

Equation (3) is utilized for the determination of $\dot{Q}_{GeO_2-red}$ at various T_{red}. The energy used to preheat the inert sweep gas and GeO_2 is not considered when calculating $\dot{Q}_{GeO_2-red}$. This is because both streams are preheated before entering the reduction cell. Because of the exclusion of the preheating of the inert sweep gas and GeO_2, the enthalpies of the individual components involved in the reduction step determine the $\dot{Q}_{GeO_2-red}$. With the rise in the T_{red} from 1600 to 2000 K, the enthalpies of GeO_2 (reactant) and GeO and O_2 (products) increase by 31.4 kJ/mol, 15.91 kJ/mol, and 15.9 kJ/mol, respectively. Figure 3 shows the impact of increasing T_{red} from 1600 to 2000 K on $\dot{Q}_{GeO_2-red}$. The results presented show that $\dot{Q}_{GeO_2-red}$ at 2000 K is 9.0 kW lower than at 1600 K. $\dot{Q}_{GeO_2-red}$ decreases when T_{red} increases from 1600 to 2000 K. This happens because the enthalpy of the reactant GeO_2 increases more than the enthalpies of the products GeO and O_2.

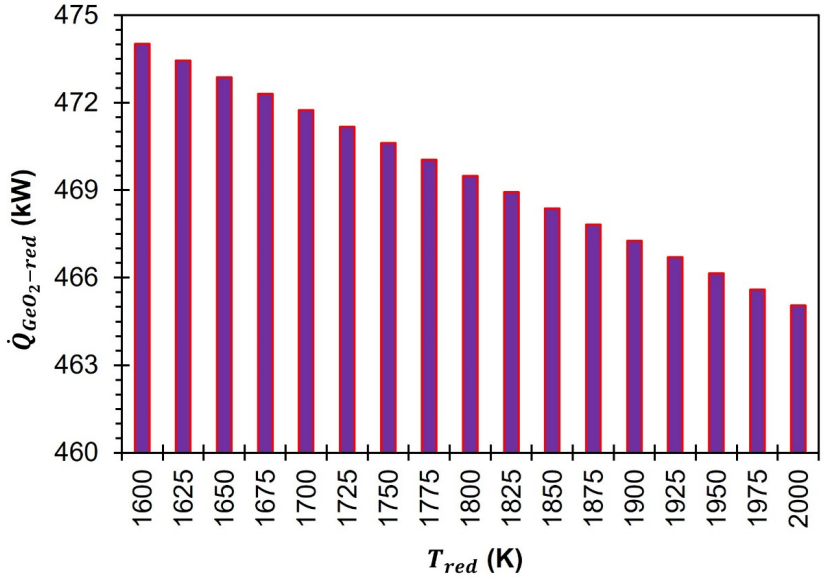

Figure 3. Variation in $\dot{Q}_{GeO_2-red}$ as a function of T_{red}.

Most studies conduct the CDS at 1000 K, according to the published literature. In addition, as per the delta G analysis (Figure 4), the CDS for the GeO_2/GeO redox cycle is feasible below 1300 K. Therefore, in this investigation the production of CO is also conducted at T_{oxd} = 1000 K via re-oxidation of GeO. With the help of HEX-1, the inert/O_2/GeO gas mixture (which exits the reduction cell) is cooled from T_{red} to T_{oxd}. This cooling process also helps to alleviate the recombination of the gaseous products O_2 and GeO. With the help of the cooling set, gaseous GeO is converted into solid GeO and separates from the mixture of inert and O_2 gases. The energy released during the cooling process is then harnessed to preheat the inert sweep gas, which helps to optimize the overall efficiency of the system. The solid GeO is transported to the oxidation cell where it undergoes a reaction with a surplus amount of CO_2, which is ten times higher than the required amount. This reaction results in the re-oxidation of GeO to GeO_2 and the production of CO through the CDS reaction. Although T_{red} varies from 1600 to 2000 K, a constant temperature of 1000 K is applied during the CDS step. Therefore, $\dot{Q}_{GeO-oxd}$ remains constant at 239.7 kW.

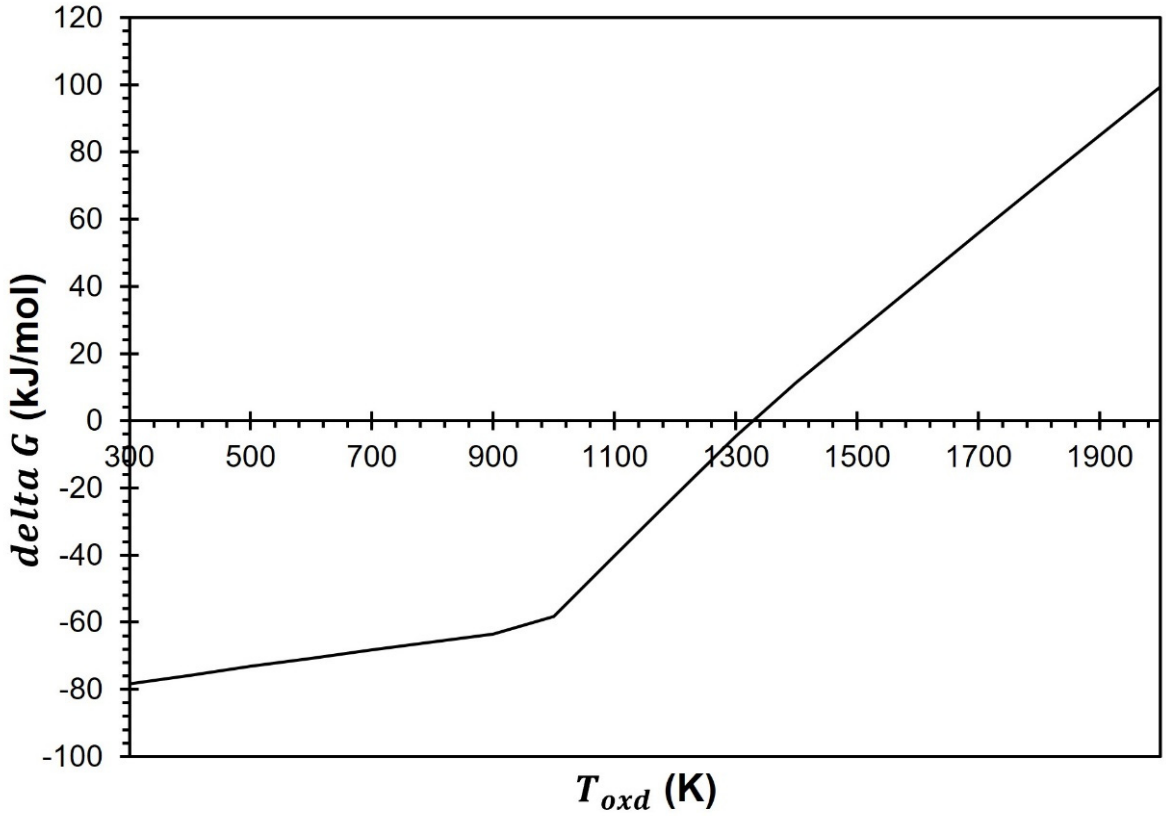

Figure 4. Variation in *delta G* as a function of T_{oxd}.

In order to ensure the around-the-clock operation of the GeO_2/GeO-based CDS cycle, it is imperative to recycle the GeO_2 generated in the oxidation cell as the feed to the reduction cell. During the re-oxidation process of GeO, it is maintained at a constant temperature of 1000 K. The resulting GeO_2 is subsequently heated to T_{red} with the aid of heater-1. This process ensures that the GeO_2 is adequately heated to the desired temperature to perform the TR step. The data presented in Figure 5 demonstrate that an increase in T_{red} from 1500 K to 2000 K results in a corresponding increase in the heat supply required from heater-1. As the T_{red} increases from 1500 K to 2000 K, $\dot{Q}_{heater-1}$ rises from 80.3 kW to 113.7 kW.

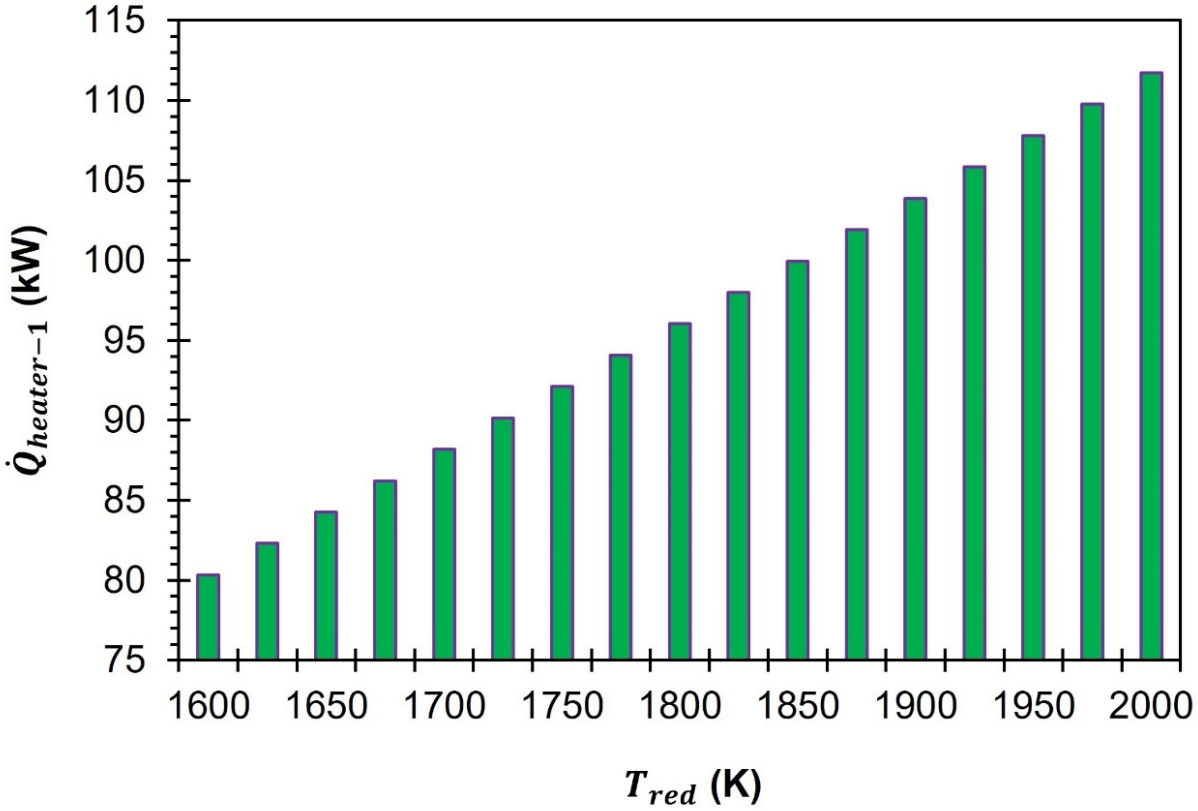

Figure 5. Variation in $\dot{Q}_{heater-1}$ as a function of T_{red}.

The oxidation cell generates a gas mixture consisting of unreacted CO_2 and CO. This gas mixture is then transferred to separator-2 for further processing. In order to reuse the unreacted CO_2 for the CDS reaction, it is necessary to separate it from CO. After separating the CO_2 from the CO, the latter is transferred to the fuel cell for the completion of the cycle. Separator-2 is operated at T_{sep-2} = 400 K. To reach the target temperature of 400 K, the mixture of CO_2 and CO gases is cooled down from 1000 K. This cooling process is made possible by HEX-4, which regulates the temperature of the gas mixture before it enters separator-2. $\dot{Q}_{sep-2}$ is estimated by using Equations (6) to (8) and by using the assumption already mentioned in the previous section. At all T_{red}, the energy required to separate CO_2 and CO remains constant at 71.8 kW. This is because changes to $\dot{n}_{CO}$ and $\dot{n}_{CO_2}$ do not change T_{red}.

To prepare for the fuel cell, the temperature of the CO is first lowered from 400 K to 298 K. This is achieved by using cooler-1, which releases heat to the ambient environment. As part of the process, the unreacted CO_2 (separated from the inert gas) also undergoes cooling, from an initial temperature of 1123 K down to 298 K. This cooling is achieved by passing the CO_2 through HEX-3. The fuel cell is a device where a chemical reaction occurs between CO and O_2. This reaction is responsible for completing the GeO_2/GeO-based CDS cycle, which ultimately leads to the production of CO_2.

The CO_2 that is generated during the operation of the fuel cell, along with the CO_2 separated from the CO, are combined and then moved to the oxidation cell. To ensure the proper functioning of the oxidation cell at 1000 K, a gas-to-gas heat exchanger, HEX-4, and an auxiliary heater, heater-4, are installed in the process. These components work together to effectively heat the CO_2 from 298 K to 1000 K, thereby facilitating the oxidation process. In the context of HEX-4, it is noteworthy that the energy that is released during the cooling process of the CO_2–CO mixture is effectively harnessed and utilized for the purpose of heating CO_2 (ε_{gg} = 0.5). To heat CO_2 from 298 K to 1000 K, more energy is required than the energy released during the cooling of a mixture of CO_2 and CO gas from 1000 K to 400 K. Therefore, an additional energy of 192.5 kW is provided by heater-4.

To keep the fuel cell running smoothly, it is crucial to maintain a constant flow of O_2. Additionally, the reduction of GeO_2 requires the presence of an inert sweep gas. The mixture of inert gas and O_2, which has been separated from GeO, requires additional separation in order to meet the aforementioned goals. To separate the O_2 from the inert sweep gas, a device called separator-1 (which is explained in detail in Section 2) is incorporated into the cycle. To separate the high-temperature stream of the inert/O_2 gas mixture, a specialized arrangement similar to an ion transport membrane separation technology is employed in the real process [36]. As per the findings published in previous studies, the most effective range for the separation of gaseous components through ion transport membranes lies in the temperature range of 1050 K to 1200 K. Therefore, in this study, separator-1 operates at 1123 K. According to the process model illustrated in Figure 1, in order to achieve T_{sep-1} of 1123 K, a mixture of inert gas and O_2 is heated with the aid of three different heating mechanisms: HEX-2, HEX-3, and heater-3 (if necessary).

In the HEX-2 and HEX-3 processes, the energy that is released during the cooling of O_2 and CO_2 is harnessed to heat up the inert/O_2 gas mixture (ε_{gg} = 0.5). According to the calculations, the amount of energy needed to heat the mixture of inert gas and O_2 is significantly greater than the sum of the energy released in the process of cooling O_2 and CO_2. To elevate the temperature of the inert/O_2 gas mixture from 1000 K to 1123 K, it is imperative to have an additional heat energy supply, which can be fulfilled by incorporating heater-3 into the system. Figure 6 displays the changes in $\dot{Q}_{heater-3}$ in response to the increase in T_{red}. It is anticipated that a particular pattern will emerge as a higher $\dot{n}_{inert}$ will be necessary to attain the full dissociation of GeO at a lower T_{red}. To achieve complete dissociation of GeO_2 at a temperature of 1600 K, it is necessary to maintain an $\dot{n}_{inert}$ of 100 mol/s, along with $\dot{Q}_{heater-3}$ = 383.5 kW. As the T_{red} is raised from 1600 K to 1700 K, 1800 K, 1900 K, and 2000 K, $\dot{n}_{inert}$ required to achieve 100% reduction of GeO_2 decreases. Specifically, $\dot{n}_{inert}$ is reduced to 73 mol/s, 44 mol/s, 14 mol/s, and 4 mol/s, respectively. As a result of the reduced demand for inert gas supply, $\dot{Q}_{heater-3}$ drops to 273.8 kW, 156.1 kW, 34.2 kW, and 0 kW, respectively.

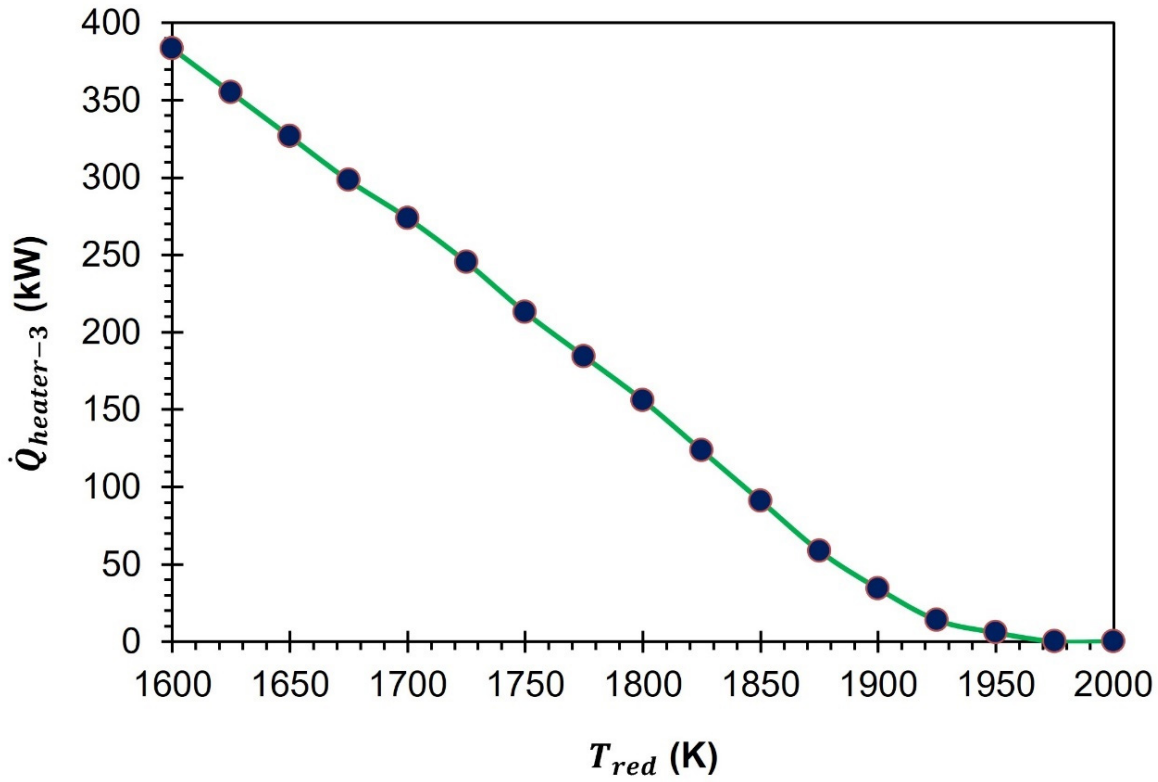

Figure 6. Variation in $\dot{Q}_{heater-3}$ as a function of T_{red}.

Upon reaching a temperature of 1123 K, the gas mixture containing inert gas and O_2 is directed towards separator-1 for further processing. By taking into account the enthalpy of mixing and applying the principles of the second law of thermodynamics, $\dot{Q}_{sep-1}$ can be estimated using Equations (16) to (18). Based on the calculations, it appears that $\dot{Q}_{sep-1}$ is significantly affected by the quantity of inert sweep gas utilized during the TR step (Figure 7). In the given scenario, it is observed that at T_{red} = 1600 K and $\dot{n}_{inert}$ = 100 mol/s, the value of $\dot{Q}_{sep-1}$ is recorded as 97.4 kW. However, as T_{red} increases to 1800 K and 2000 K, $\dot{Q}_{sep-1}$ decreases to 170.3 kW and 97.4 kW. This decrease can be attributed to the reduction in $\dot{n}_{inert}$ to 44 mol/s and 4 mol/s, respectively.

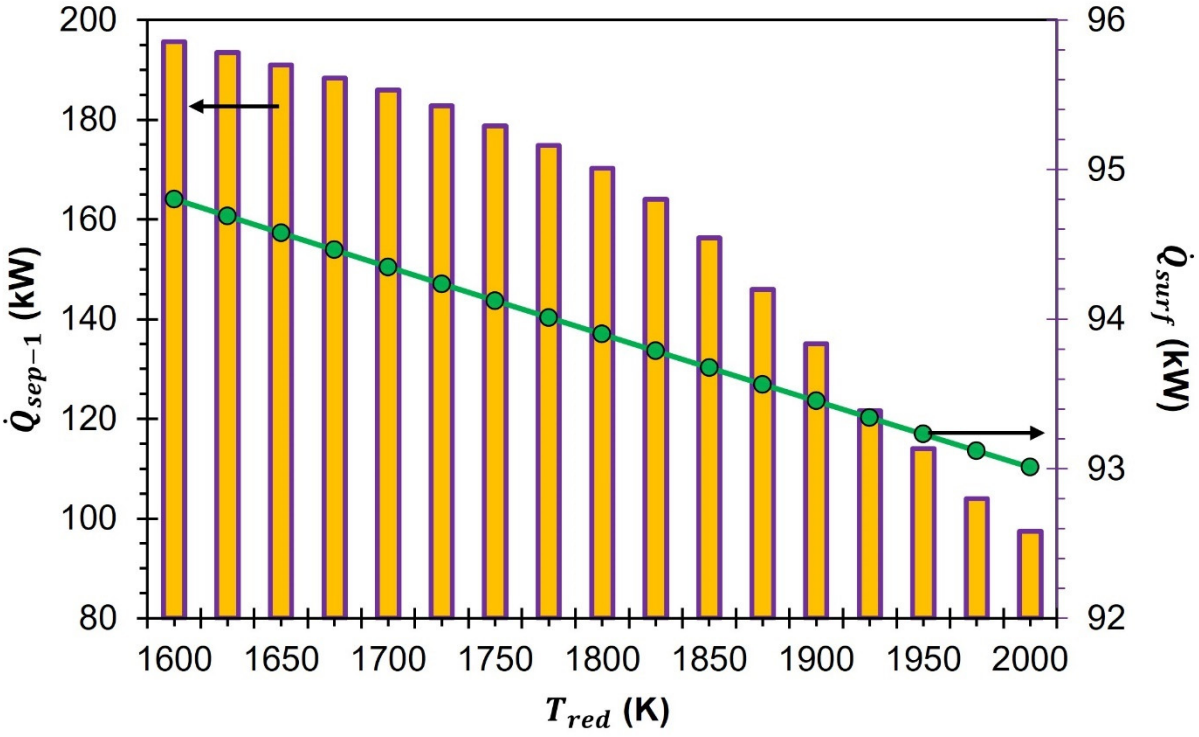

Figure 7. Variation in $\dot{Q}_{sep-1}$ and $\dot{Q}_{surf}$ as a function of T_{red}.

Once the process of separating O_2 from the inert sweep gas has been carried out successfully, the purified O_2 is directed towards the fuel cell where it engages in a chemical reaction with CO. In contrast, the inert sweep gas is subjected to further heating until it reaches T_{red} and subsequently recycled back into the reduction cell to maintain a continuous process. Within the cycle, there are two components designed to facilitate the heating of the inert sweep gas. Firstly, there is a gas-to-gas heat exchanger, also known as HEX-1. Secondly, there is a supplementary heater, aptly named heater-2, which is ready to provide additional heat to the gas if required. When the amount of energy that is recovered exceeds the amount of energy that is needed, the value for $\dot{Q}_{heater-2}$ is considered to be zero. Together, these two components enable efficient and effective heating of the inert sweep gas. The energy released during the cooling of the gaseous mixture of inert gas, O_2, and GeO is repurposed by HEX-1 to heat the inert sweep gas (ε_{gg} = 0.5). As shown in Figure 8, it can be observed that the highest $\dot{Q}_{heater-2}$ is registered at the lowest T_{red}. This is due to the requirement of using a substantial amount of inert sweep gas. It is noteworthy that the value of $\dot{Q}_{heater-2}$ is reduced by 573.9 kW when T_{red} is increased from 1600 K to 2000 K due to the reduction in $\dot{n}_{inert}$ from 100 mol/s to 4 mol/s.

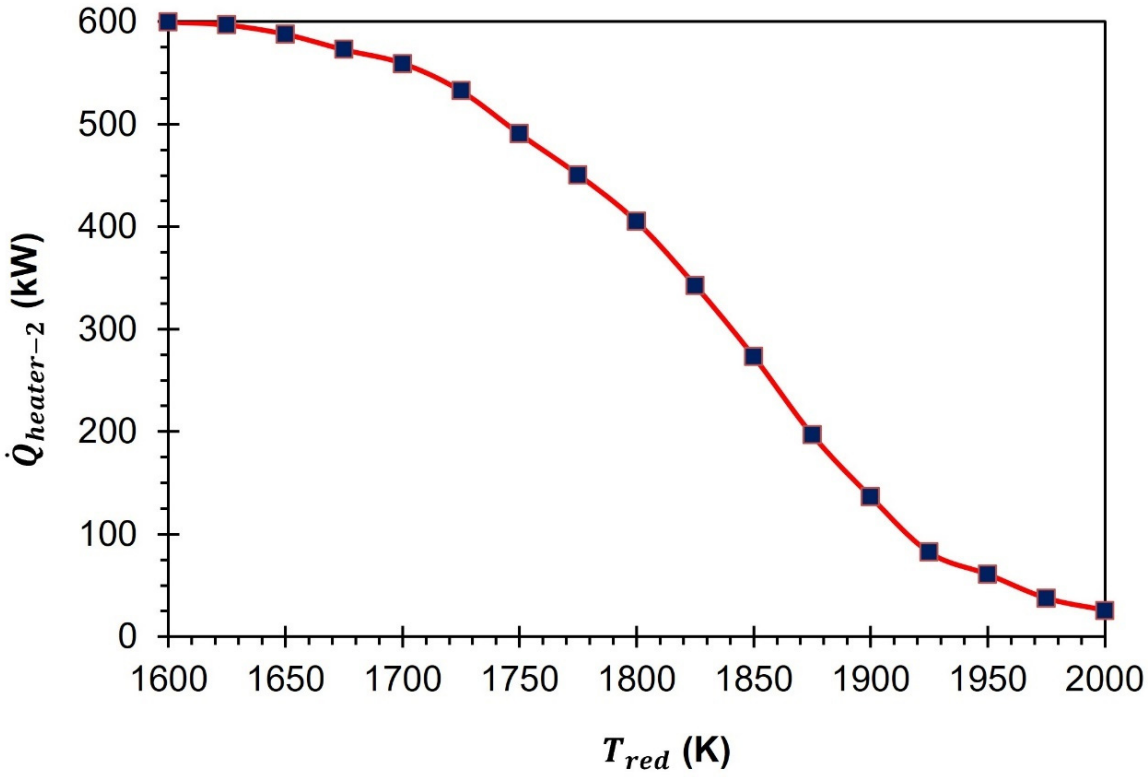

Figure 8. Variation in $\dot{Q}_{heater-2}$ as a function of T_{red}.

It is a well-known fact that heat energy tends to escape from hot surfaces through both conduction and convection. Despite the use of top-notch insulation, such losses cannot be entirely avoided. This implies that a certain amount of heat will always dissipate into the surroundings. In order to ensure accurate analysis in this study, we have taken into account the effects of conduction and convection losses. To do so, as per Equation (26), we have factored in a 20% heat loss from the surface of the reduction cell. This estimation has been derived from the findings of previously published studies on the subject [37]. As shown in Figure 7, $\dot{Q}_{surf}$ decreases from 94.8 kW to 93.0 kW when the T_{red} increases from 1600 K to 2000 K.

The amount of thermal energy needed to operate the GeO_2/GeO-based CDS cycle ($\dot{Q}_{TC}$) can be calculated using Equation (25). This equation takes into account several factors such as the energy required for the reduction reaction, as well as the heaters and separators used in the process. Additionally, any heat losses from the surface of the reduction cell are also considered in the calculation. As per the trends reported in Figure 9, $\dot{Q}_{TC}$ decreases as a function of the rise in T_{red}. At T_{red} = 1600 K, $\dot{Q}_{TC}$ is equal to 2092.5 kW. As the T_{red} increases to 1700 K, 1800 K, 1900 K, and 2000 K, $\dot{Q}_{TC}$ reduces to 1937.8 kW, 1655.1 kW, 1234.5 kW, and 1050.9 kW, respectively.

In order to understand why $\dot{Q}_{TC}$ is higher at lower T_{red}, we conducted a comparison of the total thermal energy needed for the GeO_2/GeO-based CDS cycle at two different temperatures: 1600 K and 2000 K (as shown in Figure 10). The presented results indicate that the higher $\dot{Q}_{TC}$ at 1600 K than 2000 K is mainly due to the rise in $\dot{Q}_{heater-2}$, $\dot{Q}_{heater-3}$, and $\dot{Q}_{sep-1}$. For instance, $\dot{Q}_{heater-2}$, $\dot{Q}_{heater-3}$, and $\dot{Q}_{sep-1}$ are recorded to be higher by 573.9 kW, 383.5 kW, and 98.3 kW, respectively, at 1600 K compared to at 2000 K. As previously noted, in order to sustain the operation of the cycle at a temperature of 1600 K, a considerable amount of 100 mol/s of inert sweep gas is required. This is markedly higher than the $\dot{n}_{inert}$ needed at 2000 K, which stands at 4 mol/s. The functions of heater-2 and heater-3 are to increase the temperature of the inert sweep gas in the system. On the other hand,

separator-1 is responsible for separating the inert sweep gas and O_2. As, all three units heavily depend upon the inert sweep gas flow rate, the values of $\dot{Q}_{heater-2}$, $\dot{Q}_{heater-3}$, and $\dot{Q}_{sep-1}$ are recorded to be higher at 1600 K as compared to 2000 K. In summary, it can be inferred that the primary cause for a higher value of $\dot{Q}_{TC}$ at lower T_{red} is the requirement of an excess inert sweep gas flow rate.

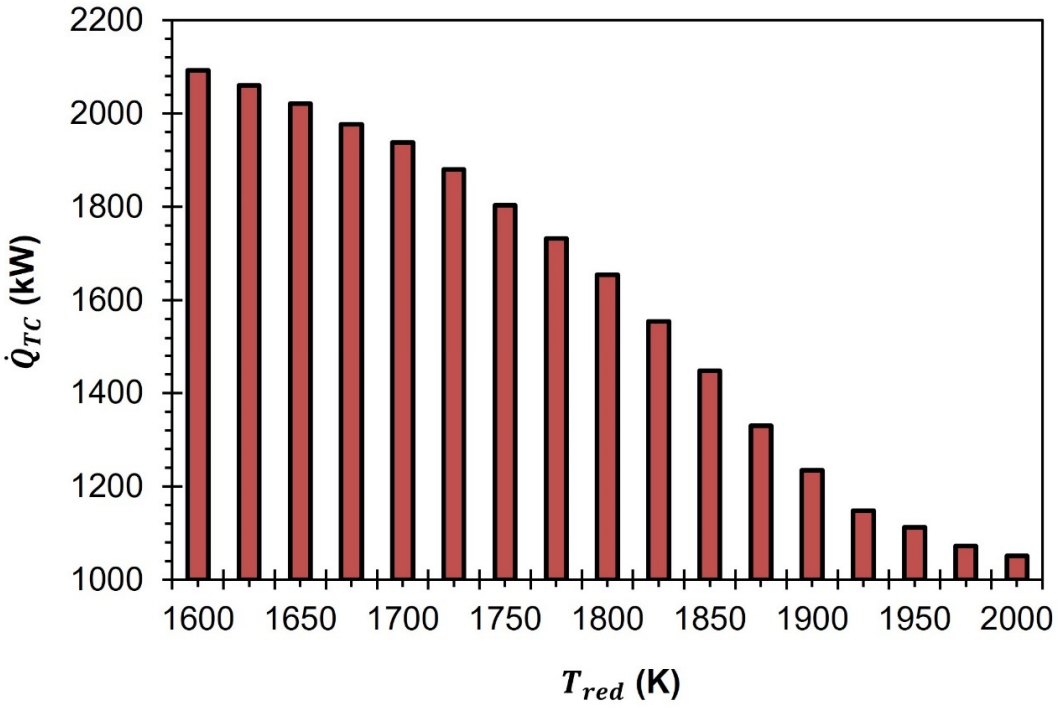

Figure 9. Variation in $\dot{Q}_{TC}$ as a function of T_{red}.

To accurately estimate the total solar energy needed for the GeO_2/GeO CDS cycle ($\dot{Q}_{solar}$), it is important to calculate the efficiency of solar energy absorption ($\eta_{absorption}$). This efficiency is highly influenced by the T_{red}, making it a critical factor to consider in the estimation process. Equation (24) is used for the estimation of $\eta_{absorption}$ by keeping $\sigma = 5.6705 \times 10^{-8}$ W/m^2·K^4, I = 1000 W/m^2, and C = 3000 suns constant. The calculations performed indicate that $\eta_{absorption}$ is higher at lower T_{red} values and as the T_{red} increases, $\eta_{absorption}$ decreases. For instance, at T_{red} = 1600 K, $\eta_{absorption}$ = 87.6% and as the T_{red} increases to 1800 K and 2000 K, $\eta_{absorption}$ reduces to 80.2% and 69.8%, respectively.

Equations (23) to (27) are used to estimate the total solar energy requirements ($\dot{Q}_{solar}$) and re-radiation losses ($\dot{Q}_{re-rad}$) for the GeO_2/GeO CDS cycle. Due to the variations in $\eta_{absorption}$ as a function of the T_{red}, $\dot{Q}_{solar}$ is observed to be different from $\dot{Q}_{TC}$. To put it differently, the $\dot{Q}_{solar}$ required to achieve a desired outcome must exceed the actual amount needed, as a portion of the energy is lost to the surrounding environment through re-radiation (Figure 11). At 2000 K, $\dot{Q}_{solar}$ is equal to 1506.6 kW, which is 455.6 kW higher than $\dot{Q}_{TC}$. As T_{red} decreases to 1600 K, similar to $\dot{Q}_{TC}$, $\dot{Q}_{solar}$ is also increased to 2388.3 kW due to the rise in $\dot{n}_{inert}$. As shown in Figure 11, $\dot{Q}_{re-rad}$ also increases from 295.8 kW to 432.7 kW due to the rise in T_{red} from 1600 K to 2000 K.

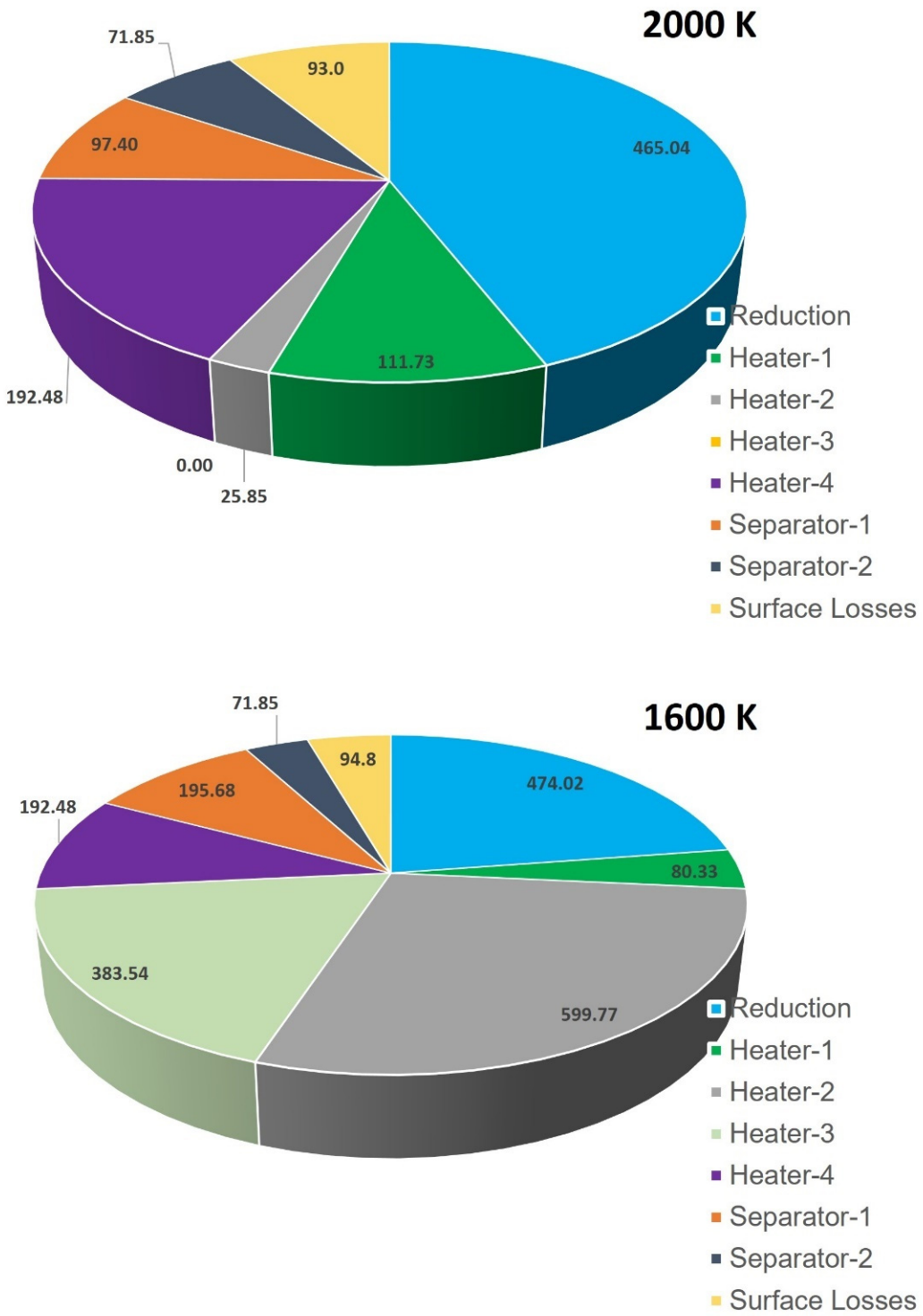

Figure 10. A comparison of $\dot{Q}_{TC}$ at two different T_{red}: 1600 K and 2000 K.

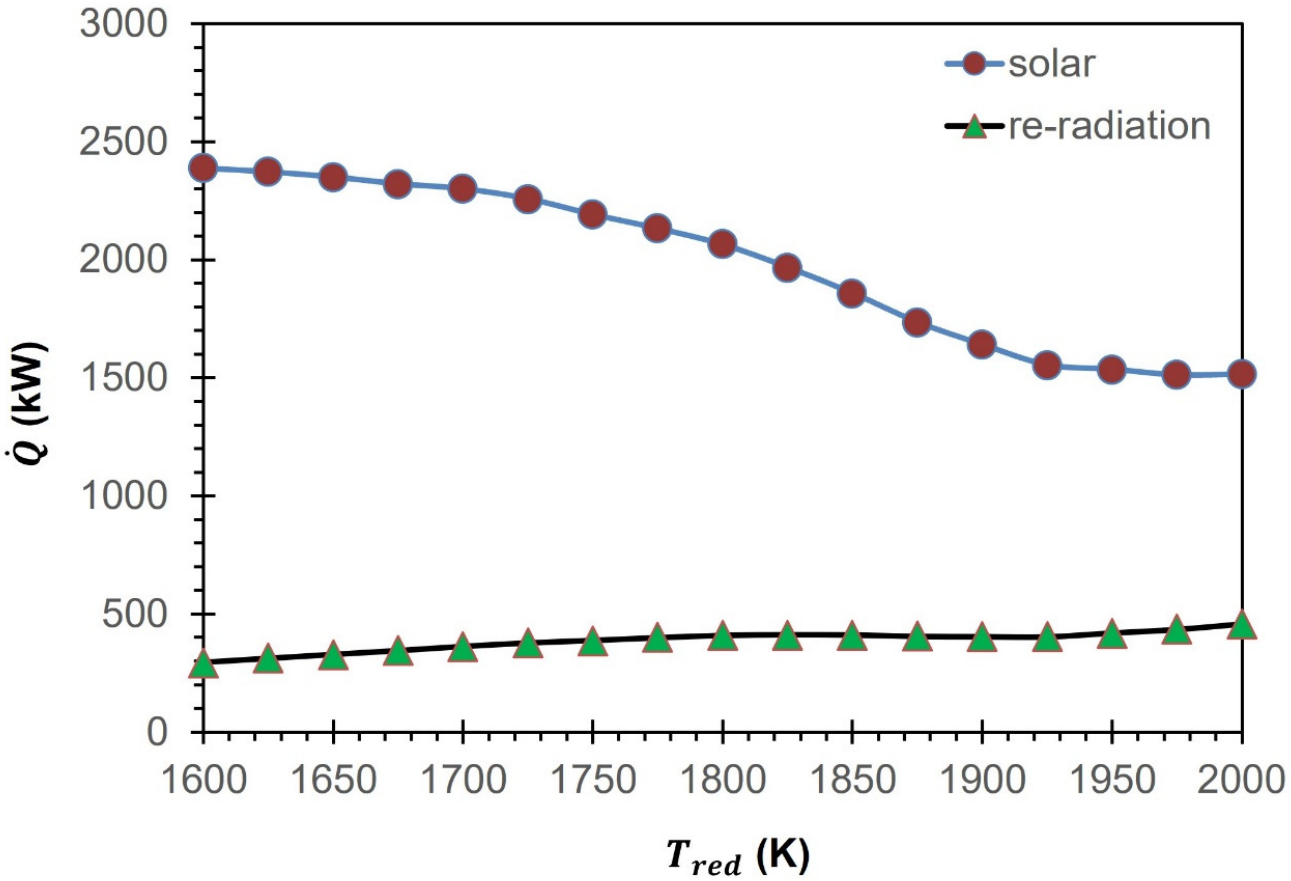

Figure 11. Variation in $\dot{Q}_{solar}$ and $\dot{Q}_{re-rad}$ for the GeO_2/GeO CDS cycle.

The $\eta_{solar-to-fuel}$ of the GeO_2/GeO-based CDS cycle is estimated using Equation (22) and presented as a function of T_{red} in Figure 12. The efficiency of converting solar energy into fuel is influenced by several factors. These factors include the quantity of produced fuel, the heating value of the fuel, and the amount of solar energy required to initiate and drive the necessary chemical reactions. The production of CO and its heating value remain constant at 1 mol/s and 283.24 kJ/mol, respectively. However, $\eta_{solar-to-fuel}$ can vary due to the change in $\dot{Q}_{solar}$ as a function of T_{red}. The findings presented in Figure 12 demonstrate that $\eta_{solar-to-fuel}$ is 11.9% when T_{red} is equal to 1600 K. However, this value increases significantly as the temperature rises. Specifically, $\eta_{solar-to-fuel}$ rises to 12.3%, 13.7%, 17.4%, and 19.2%, respectively, when T_{red} is raised to 1700 K, 1800 K, 1900 K, and 2000 K. It is interesting to note that $\eta_{solar-to-fuel}$ remains steady (19.2%) at 1975 K and 2000 K.

In Figure 13, a comparison is presented between the CDS cycles of GeO_2/GeO-based, ZnO/Zn-based [38], and SnO_2/SnO-based materials [39]. The comparison is based on the values of $\eta_{solar-to-fuel}$. According to the results presented, the $\eta_{solar-to-fuel}$ of the GeO_2/GeO cycle is higher than that of the ZnO/Zn and SnO_2/SnO cycles, at all temperatures of TR. At a temperature of 1600 K, the $\eta_{solar-to-fuel}$ of the GeO_2/GeO CDS cycle is higher than that of the ZnO/Zn and SnO_2/SnO CDS cycles by 10.5% and 11.2%, respectively. As T_{red} increases from 1600 K to 1800 K and 2000 K, the difference between the $\eta_{solar-to-fuel}$ of the GeO_2/GeO and ZnO/Zn CDS cycles reduces to 5.3% and 2.1%, respectively. In the case of the SnO_2/SnO CDS cycle, a similar trend was observed. At 1800 K, the difference between the $\eta_{solar-to-fuel}$ of the GeO_2/GeO and SnO_2/SnO CDS cycles decreases to 6.2%, and at 2000 K, it decreases to 2.4%. These results confirm that the GeO_2/GeO CDS cycle is more promising than the ZnO/Zn and SnO_2/SnO CDS cycles. The GeO_2/GeO CDS cycle is capable of achieving a reasonably high $\eta_{solar-to-fuel}$ of 10% at a temperature of less than 1600 K. On the other hand, the ZnO/Zn and SnO_2/SnO CDS

cycles require a higher operating temperature of more than 1850 K to achieve the same level of efficiency.

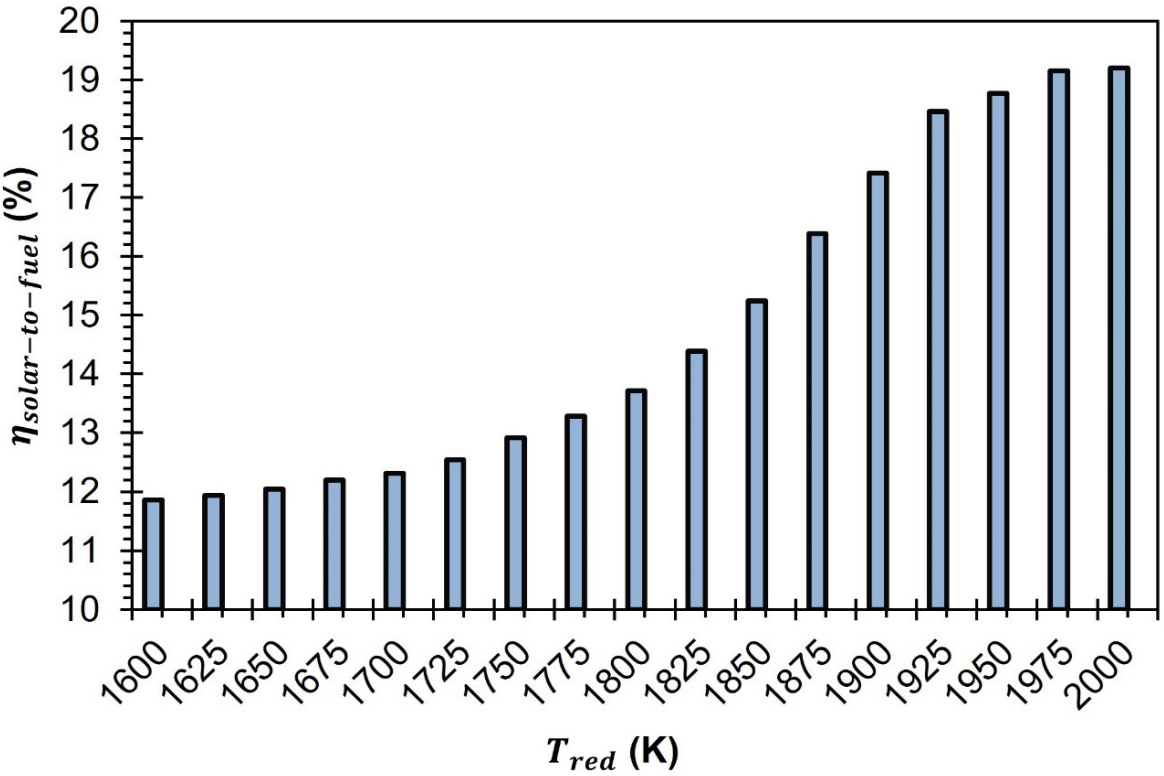

Figure 12. Variation in the $\eta_{solar-to-fuel}$ of GeO_2/GeO-based CDS cycle.

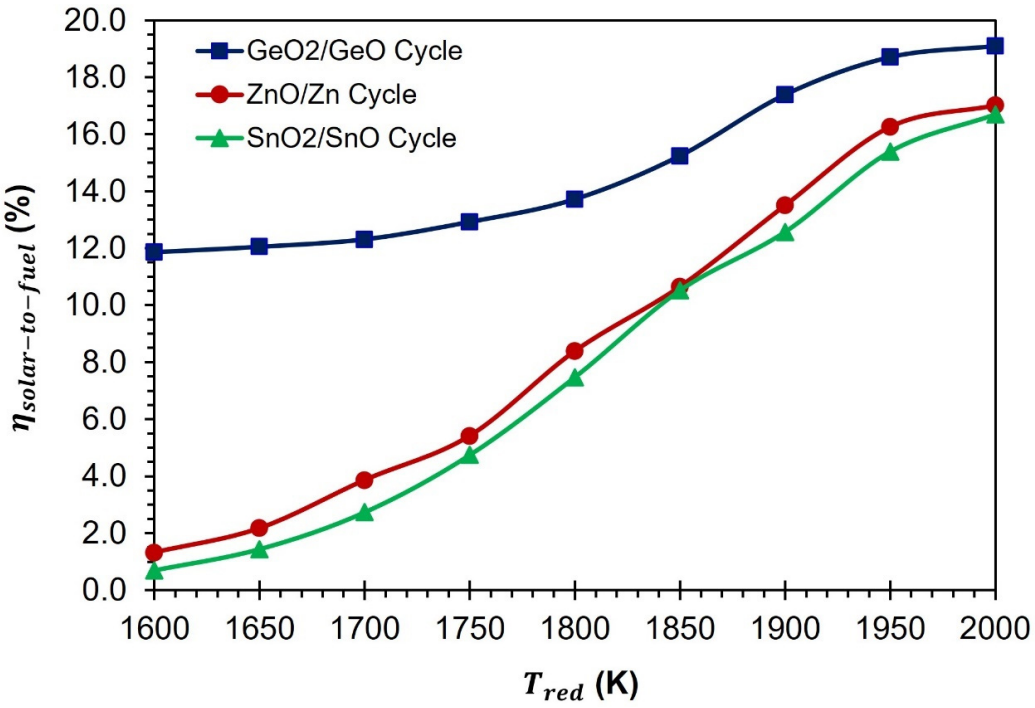

Figure 13. Comparison between the GeO_2/GeO-based, ZnO/Zn-based, and SnO_2/SnO-based CDS cycles based on $\eta_{solar-to-fuel}$.

The impressive performance of the GeO_2/GeO CDS cycle can be attributed to the lower requirement of the inert gas supply when compared to the ZnO/Zn and SnO_2/SnO CDS cycles. At 1800 K, the inert gas requirement for the GeO_2/GeO CDS cycle is lower than that of the ZnO/Zn and SnO_2/SnO CDS cycles by 51 mol/s and 89 mol/s, respectively. This reduction in inert gas flow requirement leads to a decrease in heating duty and solar energy requirements, which is reflected in a higher $\eta_{solar-to-fuel}$.

4. Summary and Conclusions

According to the equilibrium thermodynamic analysis, the $\dot{n}_{inert}$ needed for the complete thermal decomposition of GeO_2 decreases from 100 mol/s to 4 mol/s as the T_{red} rises from 1600 K to 2000 K. As the temperature of thermal reduction rises from 1600 K to 2000 K, it is observed that the enthalpies of the reactants experience a larger increase compared to the products. As a result, the energy required for thermal reduction of GeO_2 increases by 9 kW. Despite the consistent release of exothermic heat at 239.7 kW during the re-oxidation process of GeO to GeO_2 through CDS, the energy necessary to reheat the recycled GeO_2 from the oxidation cell to the reduction cell rises by 31.4 kW with an increase in T_{red} from 1600 K to 2000 K. Due to the decrease in $\dot{n}_{inert}$ at a higher T_{red} of 2000 K, the energy required to operate separator-2 decreases by 98.3 kW when the T_{red} is raised from 1600 K to 2000 K. Despite the consistent demand for 192.5 kW of supplementary energy from heater-4, the amount of energy needed from heater-3 for heating the inert/O_2 gas mixture from the re-oxidation to reduction temperature decreases from 383.5 kW to 0 kW as T_{red} increases from 1600 K to 2000 K, respectively. This is because the $\dot{n}_{inert}$ required considerably decreases with higher T_{red}. Due to the aforementioned reason, it has been observed that the overall thermal energy and the total amount of solar energy required to execute the cycle are comparatively higher at lower T_{red}. Because of the alternations associated with the solar energy requirement with a varying T_{red}, the GeO_2/GeO CDS cycle attains a lower (11.9%) and a higher (19.1%) $\eta_{solar-to-fuel}$ at 1600 K and 2000 K, respectively.

Author Contributions: Conceptualization/methodology/resources/original draft/review and editing, R.R.B.; methodology, R.R.B.; software/validation, investigation/data curation/review and editing, R.R.B., S.A.; Z.A., G.B., E.B., T.B., M.B., S.C., R.F., J.H., M.H., D.H., M.I., M.J., P.K., J.M., V.R., S.S. and J.W. All authors have read and agreed to the published version of the manuscript.

Funding: Ruth S. Holmberg Grant for Faculty Excellence, University of Tennessee at Chattanooga.

Institutional Review Board Statement: Not applicable.

Informed Consent Statement: Not applicable.

Data Availability Statement: All research data are presented in the paper.

Acknowledgments: Rahul R. Bhosale gratefully acknowledges the support provided by the Ruth S. Holmberg Grant for Faculty Excellence, University of Tennessee at Chattanooga.

Conflicts of Interest: The authors declare no conflict of interest.

Nomenclature

Variables

$\boldsymbol{n}$	Molar amount, mol
$\boldsymbol{n_{CO,O_3}}$	Molar amount of CO at state $\boldsymbol{O_3}$, mol
$\boldsymbol{n_{CO,O_4}}$	Molar amount of CO at state $\boldsymbol{O_4}$, mol
$\boldsymbol{n_{O_2,R_1}}$	Molar amount of O_2 at state $\boldsymbol{R_1}$, mol
$\boldsymbol{n_{O_2,R_2}}$	Molar amount of O_2 at state $\boldsymbol{R_2}$, mol
$\dot{\boldsymbol{n}}$	Molar flow rate, mol/s
$\dot{\boldsymbol{n}}_{\boldsymbol{inert}}$	Molar flow rate of inert gas, mol/s
$\dot{\boldsymbol{n}}_{\boldsymbol{GeO_2}}$	Molar flow rate of GeO_2, mol/s
$\dot{\boldsymbol{n}}_{\boldsymbol{GeO}}$	Molar flow rate of GeO, mol/s

$\dot{n}_{CO_2}$	Molar flow rate of CO_2, mol/s
$\dot{n}_{CO}$	Molar flow rate of CO, mol/s
$\dot{n}_{O_2}$	Molar flow rate of O_2, mol/s
$\dot{Q}_{inert-heat}$	Thermal energy required to heat inert sweep gas, kW
$\dot{Q}_{(inert+O_2)-heat}$	Thermal energy required to heat inert/O_2 gas mixture, kW
$\dot{Q}_{(inert+O_2+GeO)-cool}$	Thermal energy released during cooling of inert/O_2/GeO gas mixture, kW
$\dot{Q}_{(CO_2+CO)-cool}$	Thermal energy released during cooling of CO_2 + CO gas mixture, kW
$\dot{Q}_{CO_2-cool}$	Thermal energy released during cooling of CO_2, kW
$\dot{Q}_{CO_2-heat}$	Thermal energy required to heat CO_2, kW
$\dot{Q}_{heater-1}$	Auxiliary thermal energy required to heat GeO_2, kW
$\dot{Q}_{heater-2}$	Auxiliary thermal energy required to heat inert sweep gas, kW
$\dot{Q}_{heater-3}$	Auxiliary thermal energy required to heat inert/O_2 gas mixture, kW
$\dot{Q}_{heater-4}$	Auxiliary thermal energy required to heat CO_2, kW
$\dot{Q}_{O_2-cool}$	Thermal energy released during cooling of O_2, kW
$\dot{Q}_{solar}$	Solar energy required to run the cycle, kW
$\dot{Q}_{sep-1}$	Thermal energy required for the operation of separator-1, kW
$\dot{Q}_{sep-2}$	Thermal energy required for the operation of separator-2, kW
$\dot{Q}_{surf}$	Thermal energy losses from the walls of the reduction cell, kW
$\dot{Q}_{TC}$	Thermal energy required to run the cycle, kW
$\dot{Q}_{GeO_2-red}$	Thermal energy required for reduction of GeO_2, kW
$\dot{Q}_{GeO-oxd}$	Thermal energy released during re-oxidation of GeO, kW
$\dot{Q}_{re-rad}$	Re-radiation losses from the cycle, kW
T_0	Ambient temperature, K
T_{oxd}	Oxidation (splitting) temperature, K
T_{red}	Reduction temperature, K
T_{sep-1}	Operating temperature of separator-1, K
T_{sep-2}	Operating temperature of separator-2, K
y_{CO,O_3}	Mole fraction of CO at state O_3, mol
y_{CO,O_4}	Mole fraction of CO at state O_4, mol
y_{O_2,R_1}	Mole fraction of O_2 at state R_1, mol
y_{O_2,R_2}	Mole fraction of O_2 at state R_2, mol
$\eta_{absoprtion}$	Solar energy absorption efficiency, %
η_{sep-1}	Efficiency of separator-1, %
η_{sep-2}	Efficiency of separator-2, %
$\eta_{solar-to-fuel}$	Solar-to-fuel energy conversion efficiency, %
Abbreviations	
C	Solar flux concentration ratio, suns
HHV_{CO}	Higher heating value of CO, kJ/mol
HEX-1	Heat exchanger-1
HEX-2	Heat exchanger-2
HEX-3	Heat exchanger-3
HEX-4	Heat exchanger-4
I	Normal beam solar insolation, W/m^2
MO	Metal oxide
R	Ideal gas constant (8.314 J/mol·K)
Greek Letters	
ε_{gg}	Gas-to-gas heat recovery effectiveness
σ	Stefan–Boltzmann constant, 5.670×10^{-8} (W/m^2·K^4)

References

1. Agrafiotis, C.; Roeb, M.; Sattler, C. A review on solar thermal syngas production via redox pair-based water/carbon dioxide splitting thermochemical cycles. *Renew. Sustain. Energy Rev.* **2015**, *42*, 254–285. [CrossRef]
2. Vaidya, P.D.; Kenig, E.Y. CO_2-alkanolamine reaction kinetics: A review of recent studies. *Chem. Eng. Technol.* **2007**, *30*, 1467–1474. [CrossRef]

3. Charvin, P.; Abanades, S.; Flamant, G.; Lemort, F. Two-step water splitting thermochemical cycle based on iron oxide redox pair for solar hydrogen production. *Energy* **2007**, *32*, 1124–1133. [CrossRef]
4. Steinfeld, A.; Sanders, S.; Palumbo, R. Design aspects of solar thermochemical engineering—A case study: Two-Step water-splitting cycle using the Fe_3O_4/FeO redox system. *Sol. Energy* **1999**, *65*, 43–53. [CrossRef]
5. Loutzenhiser, P.G.; Elena Gálvez, M.; Hischier, I.; Graf, A.; Steinfeld, A. CO_2 splitting in an aerosol flow reactor via the two-step Zn/ZnO solar thermochemical cycle. *Chem. Eng. Sci.* **2010**, *65*, 1855–1864. [CrossRef]
6. Levêque, G.; Abanades, S. Thermodynamic and kinetic study of the carbothermal reduction of SnO_2 for solar thermochemical fuel generation. *Energy Fuels* **2014**, *28*, 1396–1405. [CrossRef]
7. Scheffe, J.R.; Li, J.; Weimer, A.W. A spinel ferrite/hercynite water-splitting redox cycle. *Int. J. Hydrogen Energy* **2010**, *35*, 3333–3340. [CrossRef]
8. Ackermann, S.; Takacs, M.; Scheffe, J.; Steinfeld, A. Reticulated porous ceria undergoing thermochemical reduction with high-flux irradiation. *Int. J. Heat. Mass. Transf.* **2017**, *107*, 439–449. [CrossRef]
9. Takalkar, G.; Bhosale, R.R.; AlMomani, F.; Rashid, S. Co-precipitation synthesized nanostructured Ce0.9Ln0.05Ag0.05O2−δ materials for solar thermochemical conversion of CO_2 into fuels. *J. Mater. Sci.* **2020**, *55*, 9748–9761. [CrossRef]
10. Scheffe, J.R.; Weibel, D.; Steinfeld, A. Lanthanum–Strontium–Manganese Perovskites as Redox Materials for Solar Thermochemical Splitting of H_2O and CO_2. *Energy Fuels* **2013**, *27*, 4250–4257. [CrossRef]
11. Takalkar, G.; Bhosale, R.R. Solar thermocatalytic conversion of CO_2 using PrxSr(1−x)MnO_3−δ perovskites. *Fuel* **2019**, *254*, 115624. [CrossRef]
12. Koepf, E.; Alxneit, I.; Wieckert, C.; Meier, A. A review of high temperature solar driven reactor technology: 25 years of experience in research and development at the Paul Scherrer Institute. *Appl. Energy* **2017**, *188*, 620–651. [CrossRef]
13. Charvin, P.; Abanades, S.; Lemont, F.; Flamant, G. Experimental study of SnO_2/SnO/Sn thermochemical systems for solar production of hydrogen. *AIChE J.* **2008**, *54*, 2759–2767. [CrossRef]
14. Palumbo, R.; Lédé, J.; Boutin, O.; Ricart, E.E.; Steinfeld, A.; Möller, S.; Weidenkaff, A.; Fletcher, E.A.; Bielicki, J. The production of Zn from ZnO in a high-temperature solar decomposition quench process—I. *Sci. Framew. Process. Chem. Eng. Sci.* **1998**, *53*, 2503–2517. [CrossRef]
15. Weidenkaff, A.; Steinfeld, A.; Wokaun, A.; Auer, P.O.; Eichler, B.; Reller, A. Direct solar thermal dissociation of zinc oxide: Condensation and crystallisation of zinc in the presence of oxygen. *Sol. Energy* **1999**, *65*, 59–69. [CrossRef]
16. Möller, S.; Palumbo, R. Solar thermal decomposition kinetics of ZnO in the temperature range 1950-2400 K. *Chem. Eng. Sci.* **2001**, *56*, 4505–4515. [CrossRef]
17. Steinfeld, A. Solar hydrogen production via a two-step water-splitting thermochemical cycle based on Zn/ZnO redox reactions. *Int. J. Hydrogen Energy* **2002**, *27*, 611–619. [CrossRef]
18. Haueter, P.; Moeller, S.; Palumbo, R.; Steinfeld, A. The production of zinc by thermal dissociation of zinc oxide—Solar chemical reactor design. *Sol. Energy* **1999**, *67*, 161–167. [CrossRef]
19. Weiss, R.J.; Ly, H.C.; Wegner, K.; Pratsinis, S.E.; Steinfeld, A. H_2 production by Zn hydrolysis in a hot-wall aerosol reactor. *AIChE J.* **2005**, *51*, 1966–1970. [CrossRef]
20. Funke, H.H.; Diaz, H.; Liang, X.; Carney, C.S.; Weimer, A.W.; Li, P. Hydrogen generation by hydrolysis of zinc powder aerosol. *Int. J. Hydrogen Energy* **2008**, *33*, 1127–1134. [CrossRef]
21. Perkins, C.; Lichty, P.; Weimer, A.W.; Bingham, C. Fluid-wall effectiveness for preventing oxidation in solar-thermal ZnO reactors. *AIChE J.* **2007**, *53*, 1830–1844. [CrossRef]
22. Ernst, F.O.; Steinfeld, A.; Pratsinis, S.E. Hydrolysis rate of submicron Zn particles for solar H_2 synthesis. *Int. J. Hydrogen Energy* **2009**, *34*, 1166–1175. [CrossRef]
23. Statnatiou, A.; Loutzenhiser, P.G.; Steinfeld, A. Solar syngas production via H_2O/CO_2-splitting thermochemical cycles with Zn/ZnO and FeO/Fe_3O_4 redox reactions. *Chem. Mater.* **2010**, *22*, 851–859. [CrossRef]
24. Müller, R.; Steinfeld, A. H_2O-splitting thermochemical cycle based on ZnO/Zn-redox: Quenching the effluents from the ZnO dissociation. *Chem. Eng. Sci.* **2008**, *63*, 217–227. [CrossRef]
25. Koepf, E.; Villasmil, W.; Meier, A. Pilot-scale solar reactor operation and characterization for fuel production via the Zn/ZnO thermochemical cycle. *Appl. Energy* **2016**, *165*, 1004–1023. [CrossRef]
26. Villasmil, W.; Brkic, M.; Wuillemin, D.; Meier, A.; Steinfeld, A. Pilot Scale Demonstration of a 100-kWth Solar Thermochemical Plant for the Thermal Dissociation of ZnO. *J. Sol. Energy Eng.* **2014**, *136*, 011016. [CrossRef]
27. Abanades, S.; Charvin, P.; Lemont, F.; Flamant, G. Novel two-step SnO_2/SnO water-splitting cycle for solar thermochemical production of hydrogen. *Int. J. Hydrogen Energy* **2008**, *33*, 6021–6030. [CrossRef]
28. Chambon, M.; Abanades, S.; Flamant, G. Kinetic investigation of hydrogen generation from hydrolysis of SnO and Zn solar nanopowders. *Int. J. Hydrogen Energy* **2009**, *34*, 5326–5336. [CrossRef]
29. Chambon, M.; Abanades, S.; Flamant, G. Solar thermal reduction of ZnO and SnO_2, Characterization of the recombination reaction with O_2. *Chem. Eng. Sci.* **2010**, *65*, 3671–3680. [CrossRef]
30. Abanades, S. CO_2 and H_2O reduction by solar thermochemical looping using SnO_2/SnO redox reactions: Thermogravimetric analysis. *Int. J. Hydrogen Energy* **2012**, *37*, 8223–8231. [CrossRef]
31. Kang, K.S.; Kim, C.H.; Cho, W.C.; Bae, K.K.; Kim, S.H.; Park, C.S. Novel two-step thermochemical cycle for hydrogen production from water using germanium oxide: KIER 4 thermochemical cycle. *Int. J. Hydrogen Energy* **2009**, *34*, 4283–4290. [CrossRef]

32. Bhosale, R.R. A novel three-step GeO_2/GeO thermochemical water splitting cycle for solar hydrogen production. *Int. J. Hydrogen Energy* **2020**, *45*, 5816–5828. [CrossRef]
33. Carrillo, R.J.; Scheffe, J.R. Beyond Ceria: Theoretical Investigation of Isothermal and Near-Isothermal Redox Cycling of Perovskites for Solar Thermochemical Fuel Production. *Energy Fuels* **2019**, *33*, 12871–12884. [CrossRef]
34. Dyer, P. Ion transport membrane technology for oxygen separation and syngas production. *Solid. State Ion.* **2000**, *134*, 21–33. [CrossRef]
35. Roeb, M.; Neises, M.; Säck, J.P.; Rietbrock, P.; Monnerie, N.; Dersch, J.; Schmitz, M.; Sattler, C. Operational strategy of a two-step thermochemical process for solar hydrogen production. *Int. J. Hydrogen Energy* **2009**, *34*, 4537–4545. [CrossRef]
36. Anderson, L.L.; Armstrong, P.A.; Broekhuis, R.R.; Carolan, M.F.; Chen, J.; Hutcheon, M.D.; Lewinsohn, C.A.; Miller, C.F.; Repasky, J.M.; Taylor, D.M.; et al. Advances in ion transport membrane technology for oxygen and syngas production. *Solid. State Ion.* **2016**, *288*, 331–337. [CrossRef]
37. Lu, Y.; Zhu, L.; Agrafiotis, C.; Vieten, J.; Roeb, M.; Sattler, C. Solar fuels production: Two-step thermochemical cycles with cerium-based oxides. *Prog. Energy Combust. Sci.* **2019**, *75*, 100785. [CrossRef]
38. Bhosale, R.R.; Gupta, R.B.; Shende, R.V. Thermodynamic evaluation of solar assisted ZnO/Zn thermochemical CO_2 splitting cycle. *Env. Res.* **2022**, *212*, 113266. [CrossRef]
39. Bhosale, R.R.; Shende, R.V.; Gupta, R.B. SnO_2/SnO based redox thermochemical CO_2 splitting cycle: Effect of inert gas flowrate, reduction temperature, and gas separation on the solar-to-fuel energy conversion efficiency. *Int. J. Energy Res.* **2022**, *46*, 9267–9280. [CrossRef]